SPARC X-ray diagnostics: technical and functional overview

D. Vezinet,[1] C. J. Perks,[2] E. Panontin,[2] S. Normile,[2] R. A. Tinguely,[2] J. Rice,[2] M. Reinke,[1] M. Cario,[1] J. Raimond,[1] A. Hoffmann,[1] E. Dubas,[1] A. Saltos,[1] and R. Kennedy[1]
[1)] *Commonwealth Fusion Systems, Devens MA, USA*
[2)] *Plasma Science and Fusion Center, MIT, Cambridge MA, USA*

(*Electronic mail: dvezinet@cfs.energy)

(Dated: 17 August 2024)

An overview is given of SPARC's three main X-ray diagnostics with a focus on the functions they fulfill with respect to tokamak operation. The first is an in-vessel soft X-ray tomography diagnostic, aimed at providing early-campaign information on plasma position, MHD activity and impurity content. The second is an ex-vessel set of hard X-ray scintillators aimed at detecting the presence of runaway electrons, in particular during plasma startup phases. The third is a set of X-ray Bragg spectrometers, located outside of the Tokamak Hall, aimed at informing on the ion temperature as an indirect constraint to reduce uncertainties on the fusion power, on providing plasma rotation velocity estimates and on observing impurity emission. Finally, more technical details are given on the beamlines at the end of which the spectrometers are located. It is explained how their design allows to ensure tritium containment and limiting neutron radiation while providing a straight view into the plasma that can also be used for for testing new innovative sensors.

I. CONTEXT: SPARC EARLY CAMPAIGNS

SPARC[1–3], is a new high-field medium-sized tokamak (R0=1.85 m) currently under construction by Commonwealth Fusion Systems in Devens, MA, USA. Figure 1 shows the as-built Tokamak Hall, ready for SPARC, with a focus on the East wall, ≈2.50 m thick, where multiple penetrations have been made to allow routing diagnostics equipment.

FIG. 1. SPARC Tokamak Hall. Behind the 2.50 m thick East wall lie Diagnostics Labs. X-ray lab is accessible through penetration NC4

One of SPARC's main characteristics is the use of high-temperature superconducting (HTS) coils that allow for a compact design with a high magnetic field (≈12.2 T). It aims at demonstrating a time-efficient path towards net energy production (Q>1) from a magnetically confined fusion device, and at preparing for a power plant design (ARC[4]). Its experimental plan aligns with this objective, being a mix of a steep learning curve intertwined with key milestones, outlined in[5].

The first campaign in particular comes with a steep learning curve, and the need to commission the device and reach Qfus > 1 using < 10 MW of fusion power sustained for 2-3 seconds. Later campaigns will see high neutron fluxes, with up to 140 MW of fusion power sustained for 10 seconds, with possible consequences on non-rad-hard systems.

More context on CFS's approach to peer-reviewing, on the early campaign parameters and on how the SPARC timeline impacts diagnostics design in general can be found in[6,7].

This paper focuses on introducing the 3 main X-ray diagnostics, explaining the roles they fulfill and how the burning plasma environment affected their designs. A functional and technical overview is given, and for each system another dedicated paper is refereed to, where more details can be found.

Section II shows an in-vessel Soft X-ray (SXR) tomography system that will help climb the learning curve by providing a double check on plasma position and MHD activity as well as impurity transport, but will eventually become unusable.

Section III describes a set of ex-vessel Hard X-ray (HXR) scintillators, mostly used for Runaway Electrons (RE) detection during start-up phases, but that will be able to address other phases and to convey spectroscopic information too.

Section IV focuses on a non-diagnostic subsystem: the X-ray beamlines that enable the existence of the spectrometers through penetration NC4, shown in figure 1. It is a central components of X-ray diagnostics and it is shown how the proposed components ensure tritium containment and acceptable neutron radiation levels while still providing a direct view on the plasma to multiple X-ray sensors, potentially opening opportunities for testing sensors from collaborations.

Section V depicts a set of Bragg X-ray spectrometers, installed outside of the Tokamak Hall, behind penetration NC4, providing a direct measurement of ion temperature to help constrain fusion power estimates. It will also provide a measurement of the plasma rotation velocity, and a dedicated survey spectrometer will help monitor multiple impurities.

II. IN-VESSEL SXR TOMOGRAPHY

In-vessel SXR broadband tomography is a standard diagnostic on tokamaks[8–12], commonly thought of as a multi-tool

of X-ray diagnostics. Indeed, the strong dependence of SXR emissivity on electron temperature (T_e) makes it a core-plasma quantity and originally conveyed the idea that it would offer a good proxy of T_e, thus giving insight into magnetic flux surfaces shape and position and on MHD activity[13–16]. While this is partially true, the dependence of SXR emissivity on impurity densities also means that multiple mechanisms can occasionally lead to poloidal asymmetries of SXR emissivity[17], like off-axis ICRH heating[18], strong plasma rotation[19] or also up/down asymmetries opposite to the grad B drift direction[20]. This is particularly true in plasmas containing heavy and strongly radiating impurities like W, of which most of SPARC Plasma facing Components (PFCs) are made. While it makes the interpretation of SXR emissivity maps less straightforward, it also means they convey more information than just T_e and can be used to indirectly assess impurity transport, providing valuable input for validating plasma simulations and making it a tool of choice for keeping an eye on impurity accumulation in real-time, for example.

All those uses make this diagnostic a good candidate for derisking scenario development in the early lifetime of SPARC.

The standard technology for broadband SXR sensors relies on Si-based semiconductor diodes. But these are susceptible to damage from neutron fluence, and such a system is expected to degrade very fast in a burning plasma environment[21–23]. Hence, it was decided to opt for more radiation-hard diamond-based semiconductor sensors instead.

Indeed, small chemical vapour deposition (CVD) diamonds can be used as Schottky junctions (using a boron-doped layer) for SXR detection[24–28]. They are typically ≈15 microns thick and can be used with or without bias voltage. The fact that the X-ray sensitive region (active layer) is only a few microns thick allows to manufacture very thin diamonds, which, combined with a small cross-section for neutron interaction, makes these sensors particularly resilient to neutron damage. The robustness of these sensors to high-temperatures[29] and high neutron fluences[30] has already been demonstrated, making them compatible with the first 2 campaigns of SPARC.

However, it is unlikely that both the sensors and the preamplifiers (sitting in the tokamak basement) will survive through the whole of SPARC's lifetime, hence this has to be considered as a sacrificial diagnostic that will be left as-is inside the vessel once damaged beyond use.

Significant efforts will be made to ensure SPARC can be safely operated without this SXR tomography, by carefully characterizing its synergies and correlations with other, longer-lived diagnostics (like bolometers, magnetics, UV sensors and other X-ray sensors) while all systems coexist.

As shown in figure 2, the current design has 4 identical pinhole cameras, located in port plugs, in a single common poloidal cross-section to offer a reasonable geometrical coverage and facilitate MHD interpretation. In particular, the plasma core is surveyed with a good spatial resolution. The X-points and strike points are also visible independently from the plasma core to make sure X-ray radiation localized in these regions can be properly identified (in case of fast electrons losses to the divertor for example[31]).

The interested reader will find more details in[32].

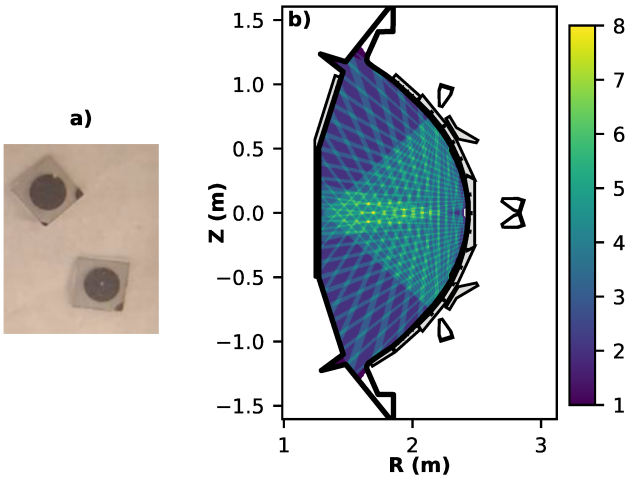

FIG. 2. (a) two 3x3 mm^2 prototype CVD diamonds (b) geometrical coverage (nb of sensors visible from each point in cross-section). Shows overlapping fields of view.

III. EX-VESSEL HXR SCINTILLATORS

During plasma start-up, high loop voltage and low density can favor the apparition of runaway electron (RE)[33,34]. A small startup RE population is both virtually unavoidable and acceptable[35]. If left unchecked however, the combination of increasing energy and population (by avalanching) can lead to RE carrying a significant fraction of the plasma current (I_P). This prevents proper ohmic heating of the bulk population to happen, and de-confined RE can locally damage PFCs[36].

Detection of start-up RE is thus critical to the operation learning curve, until robust startup scenarios are developed.

Born in the plasma[37], RE collide with ions creating thin-target bremsstrahlung. Thick-target bremsstrahlung happens when they impact PFCs. The radiation intensity depends on the RE density and energy and on the target density.

Thin-target bremsstrahlung typically happens first in time, and appears as a radiation source distributed in the plasma volume. Thick-target bremsstrahlung typically happens later but is localized on impacted PFCs, and its intensity dominates by orders of magnitude due to the much higher target density and to the typically higher energy of RE.

In both cases the radiation is peaked forward, by orders of magnitude, due to the energy of RE in the range of hundreds of keV to tens of MeV. Thin-target bremsstrahlung is equally strong all around the vessel, assuming axisymmetry of the plasma and RE population. Thick-target bremsstrahlung, on the other hand, is best detected if the sensor is located tangentially with respect to the specific PFCs impacted by RE.

SPARC has 18 discrete outer limiters. The inner limiter, on the other hand is toroidally continuous. It is not clear where exactly RE are expected to impact PFCs, as self-consistent simulations in time-varying equilibria of a growing RE population are time-consuming. But preliminary results and feedback from Alcator C-Mod and other tokamaks suggest the outer limiters are a likely target[38]. It is also a conservative hypothesis in terms of how it constrains sensor positioning.

All 18 limiters will not be monitored tangentially, but that reasonable risk is mitigated by the following considerations: particular care will be taken to properly align all limiters radially, as this is important for other reasons too, like ICRF heating, PFC erosion and resulting plasma pollution. Two distinct sensors are placed at 2 different toroidal locations, to ensure both technical redundancy and a better toroidal coverage. Also, the radiation remains significant for non-tangential views too. Finally, another type of sensor (CdTe), sensitive to 10-150 keV HXR is used with a direct view on the plasma to monitor thin-target bremsstrahlung too (see section IV).

The HXR scintillator prototypes consist of a LaBr3 cylindrical crystal of 2-3 cm in diameter and height. It is the conversion medium from HXR photons to visible light (scintillation). It is optically coupled to a photomultiplier tube (PMT) which, thanks to a photo-cathode and cascading anodes with high voltages, amplifies the detected current by 4-5 orders of magnitude. A measurable current pulse is thus issued for every HXR photon detected. A PMT was chosen over a SiPM for its better robustness vs neutron fluence, while a magnetic shield will protect it from magnetic fields of ≈200 gauss.

The HXR scintillators are located in the East wall of the Tokamak Hall, inside 2 cylindrical penetrations offering a direct, symmetrical, wide-angle view on the tokamak. Each can see RE circulating both clock-wise and anti-clockwise, depending on the scenario. Retreating the scintillators ≈50 cm into the penetration making the penetration both a collimator and a shield against the ambient neutron and gamma radiation.

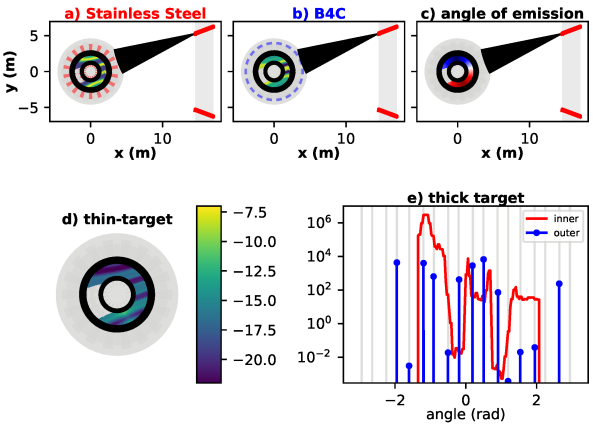

FIG. 3. (a) map of the thickness of stainless steel a photon reaching the sensor has to go through (b) thickness of B4C (c) emission angle of the photon with respect to the toroidal direction (i.e. direction of RE) (d) Total resulting contribution map, logarithmic scale (e) contribution from inner and outer limiters vs toroidal angle. The top 3 subplots have linear color bar scales.

As illustrated in figure 3, the tokamak is not an axisymmetric device for photon transport, but can instead be considered a periodic medium. In particular, the thick TF coils (red) cast a shadow inside the vessel from the point of view of a scintillator measuring > 1 MeV photons. So do the neutron shielding blocks (B4C, blue) inside the port plugs. Depending on the scintillator position, the importance of each source of signal is modulated by this pattern.

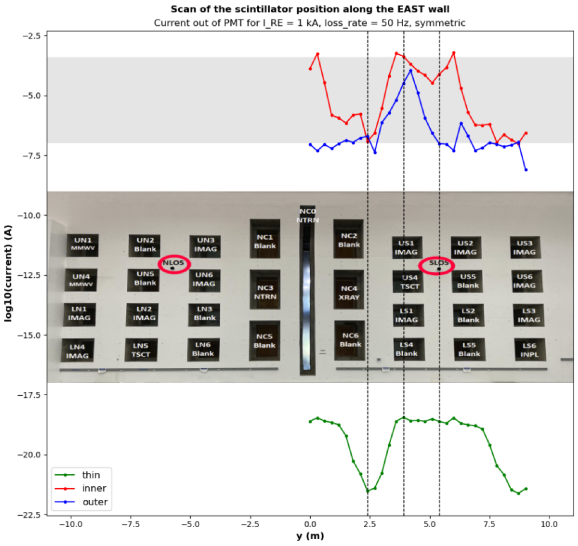

FIG. 4. Relative importance of each HXR source depending on where the scintillator is located along the East wall, the current design has them in the 2 cylindrical penetrations circled in red

As a result, one can compute which signal source is expected to be dominant (thin-target, thick target on outer limiters or in inner limiters) depending on the location of the HXR scintillator on the wall, as illustrated on figure 4.

These qualitative estimates are computed using a very simplified linear attenuation approach, and a more complete model for photon transport must be used to get an accurate quantitative computation of the synthetic signal.

The interested reader will find more details in[39,40].

IV. X-RAY BEAMLINES

As illustrated by figure 1, the East wall acts as a neutron shield between the Tokamak Hall and the Diagnostic Labs. The penetrations allow routing diagnostic equipment before they are back-filled with shielding material. Penetration NC4 is used to route 5 straight beamlines for X-ray diagnostics. They are ≈20 m long, 10 cm diameter vacuum pipes connecting the deg-0 port to a vacuum housing.

They are a diagnostic-enabling subsystem, depicted in figure 5, providing a direct view on the plasma from the Diagnostic Labs. They interface with systems like vacuum pumping, leak detection, ports, gas back-filling, and are designed to mitigate risks such as loss of tritium containment, polluting of the vessel and excess neutron radiation through the East wall.

Each beamline has a gate valve at both ends, to isolate it in case of leak. Approximately halfway, in the Tokamak Hall, each is equipped with a double vacuum window (for redundancy). X-ray vacuum windows are traditionally made out of Be, which offers the best compromise between mechanical properties (for holding pressure differences) and X-ray transparency. However, in a burning plasma environment, Be is not

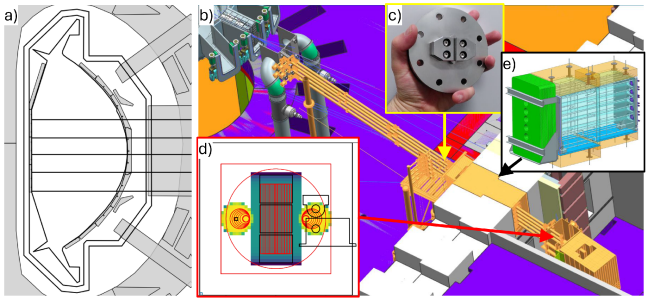

FIG. 5. (a) 5 beamlines in a poloidal projection (b) overview of the X-ray beamlines design (c) picture of a prototype vacuum window with a single diamond slit (d) projected image of the plasma through the vacuum window flange, at the sensors' location (e) design of the back-filling with shielding material

optimal as tritium tends to permeate through. It is also a neutron multiplier (x2) and tends to become brittle as it undergoes high neutron fluence, and has proven hard to procure in reasonable lead times recently. While SPARC may live with Be windows anyways, ARC is likely to be an even more demanding environment, such that it makes sense to explore ARC-relevant X-ray windows on SPARC.

Hence, SPARC has developed custom diamond windows, as CVD diamond is virtually transparent to neutrons and has low tritium permeation. It is easy to procure and thin foils (100 μm) have a reasonable X-ray transparency. It is also transparent to visible light, thus enabling laser alignment. A prototype was shown to remain leak-tight up to 12 bars.

Each window is a blank DN100CF flange holding a long central slit (for spectrometers) and 2 side pinholes. The CVD diamond foil for the central slit is pressed against an indium seal, and the 2 circular foils for the pinholes are brazed.

The image of the plasma, projected through the vacuum window flange, onto a plane perpendicular to the beamline axis and located in the vacuum housing where the X-ray sensors and crystal are located, shows the spatial arrangement of three vertically stacked crystals, two pulse height analyzers (PHA) sensors (for SXR and HXR) and an extra pinhole image for CVD sensors and possibly for testing other sensors.

V. OUT-OF-TOKAMAK HALL BRAGG SPECTROMETERS

Each beamline operates 3 different Bragg spectrometers stacked vertically, using 3 germanium crystals at very close Bragg angles. Two high-resolution spectrometers will give ion temperature (T_i) estimates, via Doppler broadening of respectively Ne-like Xe (for low-temperature plasmas) and He-like Kr lines (for high-temperature plasmas). Measuring T_i is important to assess the T_i/T_e ratio, which informs about the energy stored in the plasma and the heating power from alpha particles, thus casting light on the fusion power, as a complement to direct measurements of neutron production[41]. The third spectrometer has a lower resolution and is used to monitor multiple impurities, complementing UV spectroscopy[42].

The spectrometers live in the vacuum housing in a Diagnostic Lab, where space is shared with other systems, like the neutron spectrometer[43]. It was thus decided to go for a very compact design[44] by using a voluntarily de-focused Von Hamos configuration. The slit stands in the Tokamak Hall, close to the wall and the crystals stand in the Diagnostics Lab. The camera, instead of lying on the curvature axis of the crystals, is brought close enough to them to allow crystals and camera to live in the same unique vacuum housing. The distance is large enough for good spectral resolution and is short enough to allow projecting the images of the 3 crystals stacked together vertically on a the same common camera. This compact design, illustrated in figure 6 is possible because the use of crystals that are flat in the spectral direction does not require focusing (as opposed to being on a Rowland circle). Of course, it lowers the throughput, but greatly simplifies assembly and alignment because crystals and camera can share a common support. Also, all 3 spectrometers are time-synchronized.

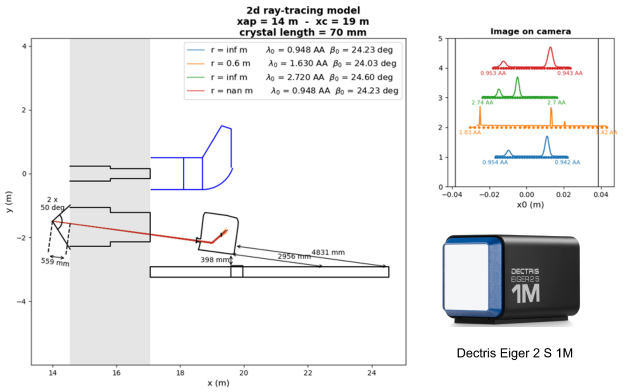

FIG. 6. (a) top-view sketch of the wall (grey) NC4 penetration (black), ray-tracing from slit to crystals to camera (red), vacuum housing (black), neutron spectrometer outline (blue). Distances to the walls are labelled. λ_0 and β_0 are the reference wavelength and bragg angle for each crystal (b) Estimated main spectra for several crystals options (c) The common camera, a DECTRIS EIGER2 S 1M[45].

The exact shape and dimensions of the crystals is not fully decided yet, the challenge being to fit all three images on the same camera without cross-talk, without losing photons out of the camera frame and without distorting the images to such an extent that it would affect spectral resolution. Several options are possible and currently under scrutiny.

The interested reader will find more details in[46].

VI. CONCLUSION

The main three X-ray diagnostics of SPARC were described, focusing on their functions and on how the burning plasma environment affected their design. System-specific solutions were found, ranging from abandon-in-place to prototyping novel custom vacuum windows, that should allow SPARC X-ray diagnostics to fulfill their roles.

VII. CONFLICTS OF INTERESTS STATEMENT

All authors are financially supported by Commonwealth Fusion Systems either as employees or through sponsored research contracts. CFS is seeking to commercialize fusion energy and may benefit financially from the science and technologies discussed in this manuscript.

ACKNOWLEDGMENTS

This work supported by Commonwealth Fusion Systems. Thanks to the broader team that supports the work of the SPARC Diagnostics systems and to the experts from institutions around the world who contributed by being external reviewers on design reviews for the SPARC X-ray diagnostics.

[1] M. Greenwald, "Status of the SPARC physics basis," Journal of Plasma Physics **86**, 861860501 (2020).
[2] A. J. Creely and et al., "Overview of the SPARC tokamak," Journal of Plasma Physics **86**, 865860502 (2020).
[3] P. Rodriguez-Fernandez and et al., "Predictions of core plasma performance for the SPARC tokamak," Journal of Plasma Physics **86**, 865860503 (2020).
[4] B. Sorbom and et al., "ARC: A compact, high-field, fusion nuclear science facility and demonstration power plant with demountable magnets," Fusion Engineering and Design **100**, 378–405 (2015).
[5] A. J. Creely and et al., "SPARC as a platform to advance tokamak science," Physics of Plasmas **30**, 090601 (2023).
[6] M. L. Reinke, B. Sorbom, and M. Greenwald, "The role of peer review in the pursuit of commercial fusion energy," Physics of Plasmas **30**, 100603 (2023).
[7] M. Reinke and et al., "Overview of the early campaign diagnostics for the sparc tokamak," Review of Scientific Instruments **these proceedings** (2024).
[8] L. C. Ingesson, B. Alper, B. J. Peterson, and J.-C. Vallet, "Tomography diagnostics: bolometry and Soft X-Ray detection," Fusion Science and Technology **53**, 528 (2008).
[9] J. F. Camacho and R. S. Granetz, "Soft x-ray tomography diagnostic for the Alcator C tokamak," Review of Scientific Instruments **57**, 417 (1986).
[10] M. Anton and et al., "X-ray tomography on the TCV tokamak," Plasma physics and controlled fusion **38**, 1849 (1996).
[11] R. Granetz and P. Smeulders, "X-ray tomography on JET," Nuclear fusion **28**, 457 (1988).
[12] A. Botrugno and et al., "Soft X-ray measurements in magnetic fusion plasma physics," Nuclear Instruments and Methods in Physics Research Section A: Accelerators, Spectrometers, Detectors and Associated Equipment **623**, 747 (2010).
[13] D. Vezinet, V. Igochine, M. Weiland, Q. Yu, A. Gude, D. Meshcheriakov, M. Sertoli, the Asdex Upgrade Team, and the EUROfusion MST1 Team, "Non-monotonic growth rates of sawtooth precursors evidenced with a new method on ASDEX Upgrade," Nuclear Fusion **56**, 086001 (2016).
[14] J. Mlynar, S. Coda, A. Degeling, B. Duval, F. Hofmann, T. Goodman, J. Lister, X. Llobet, and H. Weisen, "Investigation of the consistency of magnetic and soft x-ray plasma position measurements on TCV by means of a rapid tomographic inversion algorithm," Plasma physics and controlled fusion **45**, 169 (2003).
[15] J. Mlynar, B. Duval, J. Horacek, and J. Lister, "Present and perspective roles of soft X-ray tomography in tokamak plasma position measurements," Fusion Engineering and Design **66-68**, 905–909 (2003).
[16] J. Qian, L. Lao, Q. Ren, H. Rinderknecht, F. Volpe, C. Zhang, and B. Wan, "Equilibrium reconstruction of plasma profiles based on soft x-ray imaging in DIII-D," Nuclear Fusion **49**, 025003 (2009).
[17] R. Granetz and M. Borrás, "Is X-ray emissivity constant on magnetic flux surfaces?" Fusion engineering and design **34**, 153–157 (1997).
[18] M. L. Reinke and et al., "Poloidal variation of high- Z impurity density due to hydrogen minority ion cyclotron resonance heating on Alcator C-Mod," Plasma Physics and Controlled Fusion **54**, 045004 (2012).
[19] J. Wesson, "Poloidal distribution of impurities in a rotating tokamak plasma," Nuclear fusion **37**, 577 (1997).
[20] J. Rice and et al., en"Up/down impurity density asymmetries in C-Mod plasmas," Nuclear Fusion **58**, 126008 (2018).
[21] R. Korde, A. Ojha, R. Braasch, and T. C. English, "The effect of neutron irradiation on silicon photodiodes," Nuclear Science, IEEE Transactions on **36**, 2169–2175 (1989).
[22] A. T. Ramsey, "D-T radiation effects on TFTR diagnostics (invited)," Review of Scientific Instruments **66**, 871 (1995).
[23] J. Kohagura and et al., "Characterization of X-Ray-Energy Responses of Semiconductor Detectors After Fusion Produced Neutron Exposure," Fusion Technology **39**, 159–162 (2001).
[24] F. Bombarda and et al., "CVD diamond detectors for fast VUV and SX-ray diagnostics on FTU," Nuclear Fusion **61**, 116004 (2021).
[25] S. Cesaroni and et al., "Conceptual design of CVD diamond tomography systems for fusion devices," Fusion Engineering and Design , 6 (2023).
[26] S. Cesaroni and et al., "CVD diamond photodetectors for FTU plasma diagnostics," Fusion Engineering and Design **166**, 112323 (2021).
[27] S. Almaviva and et al., "Chemical vapor deposition diamond based multilayered radiation detector: Physical analysis of detection properties," Journal of Applied Physics **107**, 014511 (2010).
[28] I. Ciancaglioni and et al., "Influence of the metallic contact in extreme-ultraviolet and soft x-ray diamond based Schottky photodiodes," Journal of Applied Physics **110**, 054513 (2011).
[29] M. Angelone and et al., "High temperature response of a single crystal CVD diamond detector operated in current mode," Nuclear Instruments and Methods in Physics Research Section A: Accelerators, Spectrometers, Detectors and Associated Equipment **943**, 162493 (2019).
[30] M. Pillon and et al., "Radiation tolerance of a high quality synthetic single crystal chemical vapor deposition diamond detector irradiated by 14.8 MeV neutrons," Journal of Applied Physics **104**, 054513 (2008).
[31] T. Barbui and et al., "Versatile multi-energy hard x-ray camera to study confined and unconfined anisotropic characteristics of fast-electron dynamics," Review of Scientific Instruments **these proceedings** (2024).
[32] S. Normile, D. Vezinet, C. Perks, F. Bombarda, G. Verona-Rinati, and J. Rice, "Design of a diamond-based in-vessel soft x-ray detector for the sparc tokamak," Review of Scientific Instruments **these proceedings** (2024).
[33] M. Hoppe, I. Ekmark, E. Berger, and T. Fülöp, "Runaway electron generation during tokamak start-up," Journal of Plasma Physics **88**, 905880317 (2022).
[34] B. Esposito and et al., "Runaway electron generation and control," Plasma Physics and Controlled Fusion **59**, 014044 (2017).
[35] P. de Vries and et al., "Cross-machine comparison of runaway electron generation during tokamak start-up for extrapolation to ITER," Nuclear Fusion **63**, 086016 (2023).
[36] L. Ataeiseresht and et al., "Runaway electrons and their interaction with tungsten wall: a comprehensive study of effects," Scientific Reports **13**, 21760 (2023).
[37] L. F. Delgado-Aparicio and et al., en"Dynamics of runaway electron seed formation, growth and suppression in MST," (2022, 64th Annual Meeting of the APS DPP).
[38] J. Rice, *The electron distribution function and impurities in Alcator*, Ph.D. thesis, MIT (1979).
[39] E. Panontin and et al., "Development of the prototype for the sparc hard x-ray monitor," Review of Scientific Instruments **these proceedings** (2024).
[40] R. A. Tinguely and et al., "Synthetic measurements of runaway electron synchrotron emission in sparc," Review of Scientific Instruments **these proceedings** (2024).
[41] P. Raj and et al., "Overview of the preliminary design of sparc's neutron diagnostic systems," Review of Scientific Instruments **these proceedings** (2024).
[42] I. Song and et al., "Design of a multichannel vacuum ultraviolet spectroscopy system for sparc," Review of Scientific Instruments **these proceedings** (2024).
[43] S. Mackie and et al., "Ion optical design of the magnetic proton recoil neutron spectrometer for the sparc tokamak," Review of Scientific Instruments **these proceedings** (2024).
[44] D. Vezinet and et al., "Compact multiple x-ray spectrometers for SPARC," APS Division of Plasma Physics, poster (2023).

[45]Dectris, “Eiger2 s 1m documentation,”.

[46]C. Perks, D. Vezinet, J. Rice, and M. Reinke, “Performance predictions of the sparc x-ray crystal spectrometers for ion temperature and toroidal rotation measurements,” Review of Scientific Instruments **these proceedings** (2024).